Chapter 9

Colloidal suspensions

9.1 Introduction

So far we have discussed the motion of one single Brownian particle in a surrounding fluid and eventually in an extaernal potential. There are many practical applications of colloidal suspensions where several interacting Brownian particles are dissolved in a fluid.

Colloid science has a long history startying with the observations by Robert Brown in 1828. The colloidal state was identified by Thomas Graham in 1861. In the first decade of last century studies of colloids played a central role in the development of statistical physics. The experiments of Perrin 1910, combined with Einstein's theory of Brownian motion from 1905, not only provided a determination of Avogadro's number but also laid to rest remaining doubts about the molecular composition of matter. An important event in the development of a quantitative description of colloidal systems was the derivation of effective pair potentials of charged colloidal particles. Much subsequent work, largely in the domain of chemistry, dealt with the stability of charged colloids and their aggregation under the influence of van der Waals attractions when the Coulombic repulsion is screened strongly by the addition of electrolyte. Synthetic colloidal spheres were first made in the 1940's. In the last twenty years the availability of several such reasonably well characterised "model" colloidal systems has attracted physicists to the field once more. The study, both theoretical and experimental, of the structure and dynamics of colloidal suspensions is now a vigorous and growing subject which spans chemistry, chemical engineering and physics.

A colloidal dispersion is a heterogeneous system in which particles of solid or droplets of liquid are dispersed in a liquid medium. Familiar examples of such systems include industrial and household products such as paints and inks, food products such as mayonnaise and ice cream, and biological fluids such as blood and milk. Colloidal dispersions are characterised by an extremely high area of interface; for example, in a 5 litre tin of emulsion paint, which essentially consists of polymer spheres of 200 nm radius dispersed in water, the total area of interface between water and polymer is around 15000 m^2. Associated with this area of interface is a substantial amount of interfacial energy, and one has to ask the question why the polymer particles do not combine to form larger aggregates to reduce this interfacial energy. Thus understanding the stability or otherwise of a colloidal dispersion is a central issue. Gravity is one force which may destabilise a dispersion; if the dispersed particles are less dense than the dispersing fluid, they will tend to rise to the

surface, or cream, as indeed the fat droplets in untreated full-cream milk will tend to do. A denser dispersed phase, in contrast, will tend to sediment. Opposing this tendency is the Brownian motion of the particles; as the dispersed particles become smaller the size of the gravitational force decreases until it may be in effect overcome by the random thermal motion of the particles. Fullcream milk is homogenised by forcing it through a small nozzle to reduce the size of the fat globules. If the particles are small enough to minimise the effect of gravity in destabilising the dispersion, we still need to consider what happens if particles are able to collide with each other in the course of their random, Brownian motion.

When colloidal particles are able to come into contact they will stick together irreversibly. As time goes on larger and larger assemblies of particles will be formed in a process known as aggregation. If we are to render a colloidal dispersion stable against aggregation, we must modify the forces acting between the colloidal particles, which are normally attractive, to make the particles repel each other. This can be done by exploiting electrostatic forces. in charge stabilisation, or by modifying the interfaces by attaching polymer chains to them, in steric stabilisation.

Particles can be regarded as colloids if they have radii R in the range $1\text{nm} < R < 500\text{nm}$, although any such definition is inevitably imprecise. The lower limit comes from the requirement that the particles be significantly larger than the molecules of the suspension medium. The upper limit ensures that the particles' Brownian motion is not dominated by extraneous effects such as gravitational settling (or rising) or convection. Typically, then, a colloidal particle is some 100 times larger than an atom. This disparity of size has several important consequences. Firstly, while the number density n of an atomic material is $\simeq 5\times10^{22}\text{cm}^{-3}$, that of a typical colloidal suspension is $\simeq 5\times10^{13}\text{cm}^{-3}$. Since the strength of a solid is proportional to n and the potential energy, per particle, of interaction is similar in each case, colloidal crystals and glasses are around 100 times weaker than their atomic counterparts. Secondly we can define a "structural relaxation time" τ_R for a fluid material by

$$\tau_R = \frac{R^2}{D}$$

where D is an appropriate self-diffusion coefficient of a particle; τ_R is the time taken by the particle to diffuse a distance equal to its radius. For an atomic material $\tau_R \approx 2\times10^{-11}$ s whereas for a typical colloid $\tau_R \approx 2\times10^{-2}$ s. The weakness of colloidal solids means that they can easily be disrupted, or melted, by the action of relatively weak forces such as those induced by a shear flow in the suspension. The large relaxation times mean that, once shear-melted, a colloidal system will take a macroscopic time (seconds, minutes or even hours) to recrystallise. Thus well-defined metastable (nonequilibrium) states of colloidal systems, having lifetimes long enough to allow their experimental study, can be readily prepared.

The colloid analogue of an atomic fluid's pressure P is the osmotic pressure Π (thus van't Hoff's low-concentration law $\Pi = nk_\text{B}T$ is equivalent to the equation of state of an ideal gas). The osmotic pressure of suspensions of particles, e.g., proteins, at the lower end of the colloidal size range, for which n is large, can be measured quite accurately. However for $R \geq 50$ nm, say, measurement of the osmotic pressure is beyond current experimental capability, except for particles interacting very strongly or for suspensions at high concentrations.

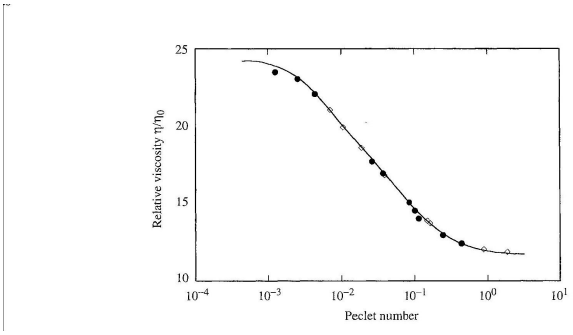

Figure 9.1: *Relative viscosity as a function of shear rate for model hard-sphere particles. The shear rate $\dot{\gamma}$ is plotted as the dimensionless combination, the Peclet number $P_e = 6\pi\eta_0 R^3\dot{\nu}/k_{\mathrm{B}}T$. The solid line is for polystyrene particles of radii between 54 and 90 nm in water. The circles are 38 nm polysterene particles in benzyl alcohol, and the diamonds 55 nm polystyrene spheres in meta-cresol.*

An important difference between atoms and colloids concerns the latter's size distribution. The atoms (of one isotope) of a particular element are identical. However, with the possible exception of some biological materials, colloidal particles inevitably have some distribution of size or *polydispersity*. A useful index σ of the polydispersity of spherical particles is the standard deviation of the particle size distribution $P(R)$ divided by its mean:

$$\sigma = \frac{\left[\overline{R^2} - \overline{R}^2\right]^{1/2}}{\overline{R}}$$

where

$$\overline{R^n} = \int \mathrm{d}R R^n P(R)$$

In the best cases synthetic particles can be prepared with $\sigma < 0.01$. Frequently polydispersities of 0.05 or larger must be tolerated. Strictly, then, a multi-component approach should be applied to colloidal systems. However common sense suggests that an effective one-component approach should be adequate for sufficiently narrow distributions. In radiation scattering experiments polydispersities as small as 0.05 can significantly affect both total intensity and dynamic measurements.

The most commonly-used variable to describe the concentration of a colloidal suspension is ϕ, the fraction of the total sample volume which is occupied by the particles. For a monodisperse system this "volume fraction" is

$$\phi = \frac{4}{3}\pi R^3 n$$

whereas for a polydisperse suspension

$$\phi = \frac{4}{3}\pi \overline{R}^3 n$$

The essentially macroscopic relaxation time τ_R has important consequences for suspension rheology. A shear flow in a fluid will change its microstructure from that obtaining at equilibrium. In an atomic fluid, where experimentally attainable shear rates $\dot{\nu}$ are much smaller than the intrinsic relaxation rate τ_R^{-1}, perturbation of the equilibrium structure is very small. The fluid is therefore Newtonian, its viscosity being essentially independent of shear rate. By contrast, in suspension rheology shear rates which exceed τ_R^{-1} are easily achieved. As a consequence colloidal suspensions show a rich variety of technologically-important non-Newtonian behaviour. Considerable current effort is being devoted to determining the connections between the macroscopic rheological properties of suspensions and their microscopic non-equilibrium structures.

In fig 9.1 the viscosity is plotted as a function of shear rate or Peclet number

$$P_e = \frac{6\pi\eta_0 R^3}{k_{\mathrm{B}}T}\dot{\nu}$$

where η_0 is the viscosity of the fluid. The plot has a very characteristic shape, with a transition from a limiting viscosity at low shear rates to a lower limiting value at high shear rates. The transition occurs over a broad range of shear rates, two or three orders of magnitude, but the onset of the high shear rate limit is characterised by a Peclet number of order unity.

The dependence of the viscosity on volume fraction for model hard sphere colloids is shown in fig. 9.2 for both the high and low shear rate limits. At the lowest volume fractions no shear rate dependence is detectable, and the Einstein relation

$$\eta = \eta_0(1 + 2.5\phi) \tag{9.1}$$

is obeyed. At higher volume fractions, the high shear rate relative viscosity can be fitted to the function

$$\eta_{\mathrm{high}} = \eta_0 \left(1 - \frac{\phi}{0.71}\right)^{-2} \tag{9.2}$$

At low shear rates a similar function

$$\eta_{\mathrm{low}} = \eta_0 \left(1 - \frac{\phi}{0.63}\right)^{-2} \tag{9.3}$$

provides a good fit. The most striking feature of the viscosities at both high and low shear-rate limits is that they appear to diverge at a finite volume fraction. In the low shear rate limit, the volume fraction, 0.63, at which the viscosity appears to diverge corresponds quite closely to the volume fraction for random close packing of hard spheres, which is $\phi = 0.64$. At slightly lower volume fractions than this we would expect this divergence in viscosity to lead to a glass transition, and indeed it is found that random hard-sphere colloids with volume fractions between about 0.58 and the random close-packing limit form long-lived metastable states, rather than ordering to the thermodynamically favoured, lower free energy, close-packed crystal. The higher volume fraction marking the divergence in the high shear. rate limit is closer to the volume fraction for a close-packed crystal at $\phi = 0.7404$. This must reflect an ordering induced by the shear flow at these higher shear rates.

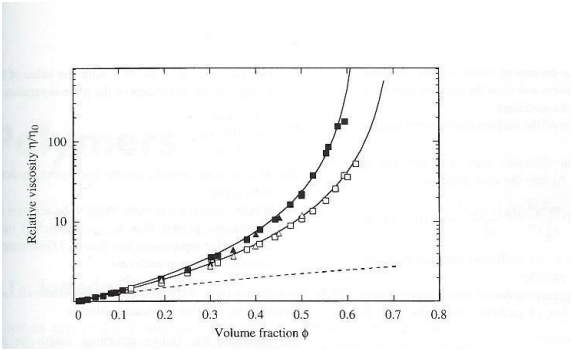

Figure 9.2: *Relative viscosity as a function of volume fraction for model hard spheres, in the limit of low shear rates (filled symbols) and high shear rates (open symbols). The solid lines are the fitting functions in (9.2) and (9.3) respectively. The dashed line is the Einstein prediction for the dilute limit in (9.1). Squares are 76 nm silica spheres in cyclohexane and triangles are polysterene spheres of radii between 54 and 90 nm in water.*

9.2 Interparticle forces

To describe a system of interacting Brownian particles a potential of mean force $U(\boldsymbol{r}^N)$ which depends, in general in a complicated fashion, on the positions $\boldsymbol{r}^N = \{\boldsymbol{r}_1, \boldsymbol{r}_2, \ldots, \boldsymbol{r}_N\}$ of all the colloidal particles. To make progress it is usually assumed that U can be written as the sum of a pair potentials $V(\boldsymbol{r}_j - \boldsymbol{r}_k)$, which, for spherical particles, are taken to be spherically symmetrical, so that

$$U(\boldsymbol{r}^N) = \sum_{j>k} V(\boldsymbol{r}_j - \boldsymbol{r}_k) \tag{9.4}$$

strictly V should be called the "effective pair potential of mean force". Equation (9.4) implies that the interaction between particles j and k is not affected by the presence of other particles. For short-ranged interactions, such as those of hard spheres, this is clearly a reasonable assumption. For forces of longer range its validity is doubtful. For example, in the case of the screened Coulombic interaction of charged particles, the proximity of a third particle will almost certainly distort the counterion atmospheres, and thereby affect the interaction, of particles j and k. There is little, if any, direct experimental evidence of the breakdown of the pairwise additivity assumption (9.4).

9.2.1 Van der Waals attraction

Between any two bodies, of matter there is a force caused by the interaction between the fluctuating electromagnetic fields associated with their polarisabilities. This force is attractive and is known as the dispersion, van der Waals or London-van der Waals force. The attraction between two atoms separated by distance r goes as r^{-6} and the interaction between two particles of radius R, obtained by summing over all pairs of atoms, is

$$V_A(r) = \frac{A}{6}\left[\frac{2R^2}{2r^2 2 - 4R^2} + \frac{2R^2}{r^2} + \ln\left(1 - \frac{4R^2}{r^2}\right)\right] \tag{9.5}$$

where r is now the centre-to-centre separation. The Hamaker constant A is determined by the material properties of the particles and suspension medium, in particular their frequency-dependent polarisabilities; a typical value of A is 10^{-20} J. Of future relevance is the fact that if the particles and liquid have equal polarisabilities, $A = 0$. Thus if the refractive indices of the particles and liquid are matched at the frequency of visible light, van der Waals attractions are expected to be negligible (or at least small since some difference in polaris abilities may obtain at other frequencies). For large interparticle separations the r^{-6} behaviour is recovered, as expected,

$$\lim_{r\to\infty} V_A(r) = -\frac{16}{9} A \left(\frac{R}{r}\right)^6 . \tag{9.6}$$

When the spheres are close to touching,

$$\lim_{r\to 2R} V_A(r) = -\frac{A}{12}\frac{R}{r-2R}. \tag{9.7}$$

In principle, therefore, the attractive potential at touching, $r = 2R$, is infinite. In reality the steep Born repulsion, due to the overlap of electron clouds, intervenes. Furthermore, solvation forces, associated with the finite size of the liquid molecules, become important at small separations. Nevertheless the effect of van der Waals forces is to create a deep potential minimum near $r = 2R$ which can be many times greater than the thermal energy $k_{\mathrm{B}}T$. Suspended particles which are unprotected will soon aggregate irreversibly under the influence of these strong attractions. It is therefore necessary to provide some stabilisation mechanism which provides a large positive potential barrier in $V(r)$. Two approaches are common, charge and steric stabilisation.

Electrostatic double-layer forces

Charged colloidal particles can be regarded as "macroions". On their surfaces are ionisable groups at least some of which dissociate when the particles are dispersed in a polar liquid such as water. The particles thus acquire a charge, typically 10^2 to 10^5 elementary charges e. The counterions discharged into the liquid move away from the macroion in Brownian motion but nevertheless remain in its field of force. The result is an electrical double layer surrounding the particle, composed of the counterions and the ions of any electrolyte present in the suspension. When two macroions approach each other, overlap of their double layers causes a repulsive force which can stabilise the particles against aggregation.

Rather than a direct Coulomb interaction between two charged particles, one finds a screened Coulomb interaction which exponentially decays in strength with distance. Suppose our particles are ionised. Overall charge neutrality will be maintained by a layer of counterions which will be attracted to the surface by the electrostatic field. Some of these counterions may be tightly bound to the surface (this layer of tightly bound ions is known as the Stern layer), but more will form a diffuse concentration profile away from the surface. There will be an electrostatic potential $V_C(\boldsymbol{r})$ at a distance r from the particle, and the density of ions $n(r)$ will be determined by the Boltzmann distribution

$$n(\boldsymbol{r}) = n_0 \exp\left(-\frac{zeV_C(\boldsymbol{r})}{k_{\mathrm{B}}T}\right)$$

where the charge of the ions is ze.

Now the potential $V_C(\boldsymbol{r})$ is itself determined by the distribution of net charge $\rho(r)$ by the Poisson equation

$$\nabla^2 V_C(\boldsymbol{r}) = -\frac{\rho(\boldsymbol{r})}{\epsilon\epsilon_0} \tag{9.8}$$

where ϵ_0 is the dielectric constant in vacuum, and ϵ the relative dielectric constant. In the simplest case where the only ions present are the counterions needed to balance the charge of the surface, $\rho = zen$, and we can combine these two equations to give the Poisson- Boltzmann equation:

$$\nabla^2 V_C(\boldsymbol{r}) = -\frac{zen(\boldsymbol{r})}{\epsilon\epsilon_0} \tag{9.9}$$

In general we have both negative and positive ions to consider. Taking these concentrations to be n_+ and n_- we have

$$n_\pm(\boldsymbol{r}) = n_0 \exp\left(\mp\frac{zeV_C(\boldsymbol{r})}{k_\mathrm{B}T}\right)$$

where n_0 is the ionic concentration in bulk solution. The net charge density is given by

$$\rho = ze(n_+ - n_-)$$

so assuming spherical symmetry

$$\frac{1}{r^2}\frac{\mathrm{d}}{\mathrm{d}r}\left(r^2\frac{\mathrm{d}}{\mathrm{d}r}V_C(r)\right) = \frac{2zen_0}{\epsilon\epsilon_0}\sinh\left(\frac{zeV_C(r)}{k_\mathrm{B}T}\right). \tag{9.10}$$

Let $V_C(r) = u(r)/r$, i.e $\mathrm{d}V_C(r)/\mathrm{d}r = -u(r)/r^2 + u'(r)/r$, and so $r^2V'(r) = -u(r) + ru'(r)$. This leads to

$$\frac{\mathrm{d}^2}{\mathrm{d}r^2}u(r) = \frac{2zen_0}{\epsilon\epsilon_0}r\sinh\left(\frac{zeu(r)}{k_\mathrm{B}Tr}\right) \approx \frac{2z^2e^2n_0}{\epsilon\epsilon_0 k_\mathrm{B}T}u(r) \tag{9.11}$$

where we have made the approximation $\sinh(zeu(r)/k_\mathrm{B}T) \approx (zeu(r)/k_\mathrm{B}Tr)$. In this limit (known as the Debye-Hückel approximation) (9.11) has the solution

$$V_C(r) = \frac{u(r)}{r} = \frac{q_e^2}{\epsilon\epsilon_0 r}\mathrm{e}^{-\kappa r} \tag{9.12}$$

where q_e is the effective charge on the macroion, and κ has the value

$$\kappa = \left(\frac{2z^2e^2n_0}{\epsilon\epsilon_0 k_\mathrm{B}T}\right)^{1/2} \tag{9.13}$$

There is also an increasing solution to (9.11) but this has to be rejected since the potential has to approach zero as $r \to \infty$.

Thus in an electrolyte, electric fields are *screened*. The length which characterises this screening, κ^{-1}, is known as the *Debye screening length*. At distances much greater than the Debye screening length, which is inversely proportional to the square root of the concentration of salt in the electrolyte, the strength of the direct electrostatic interaction between charged objects rapidly falls to zero.

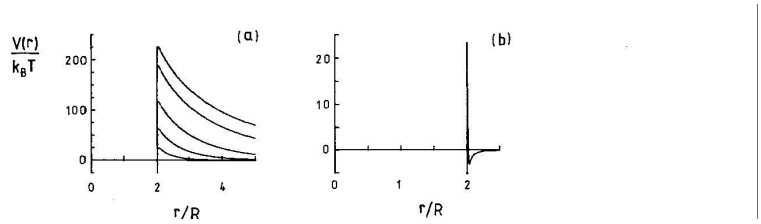

Figure 9.3: *Effective potential $V(r)$, the sum of the van der Waals attraction, eq. (9.6), and the Coulombic repulsion, for charged particles. (a) Radius $R = 50$ nm, charge $q_e = 200$ e, Hamaker constant $A = 10^{-20}$ J, temperature $T = 293$ K, relatively low electrolyte concentration giving screening parameters κ such that $\kappa R = 0.1$(top curve), 0.2, 0.5, 1,2 (bottom curve). (b) $R = 500$ nm, $q_e = 5 \times 10^4 e$, $A = 10^{-20}$ J, $T = 293$ K, moderate electrolyte concentration giving $\kappa R = 123$. In each case note the primary minimum at touching (interparticle separation $r = 2R$) and maximum at slightly larger r. In (a) the van der Waals attraction has negligible effect at separations somewhat greater than $2R$.*

The effective pair interaction of charged macroions becomes:

$$V_C(r) \begin{cases} 0 & 0 < r < 2R \\ \frac{q_e^2}{\epsilon\epsilon_0 r} \mathrm{e}^{-\kappa r}, & r > 2R \end{cases} \tag{9.14}$$

The total pair potential $V(r)$ of charged particles is the sum of the van der Waals attraction $V_A(r)$ and the Coulombic repulsion $V_C(r)$. Typically $V(r)$ has the form sketched in fig. 9.3. For $r \approx 2R$ the attraction dominates and $V(r)$ has a deep "primary" minimum. Except in the case of small macroion charge and/or large screening parameter κ the repulsion dominates at somewhat larger r, providing a maximum in $V(r)$. For the suspension to be stable for a reasonable length of time against aggregation q_e and κ must be such that the maximum in $V(r)$ is greater than about $20 k_\mathrm{B} T$. Finally, at larger r, since V_A decays as r^{-6} and V_C decays exponentially, $V(r)$ shows a secondary minimum.

Steric stabilisation

Steric stabilisation is achieved by coating colloidal particles with layers of polymer. Many types of "polymer" may be used for this purpose, ranging from relatively short alkane chains through various more complex structures to essentially random coils. The coating may be physically adsorbed on the particle or chemically bonded to it. Because of the wide variety of systems (particles, polymer, solvent) encountered it is not possible to give a theory of steric stabilisation which has the same generality as that of charge stabilisation. The close approach of two coated particles causes compression of their interpenetrating polymer layers. The resulting strong repulsive force provides the steric stability. At somewhat larger interparticle separations, where layer interpenetration is still significant, more specific polymer-polymer interactions can be important. For random-coil polymers these interactions can be attractive or repulsive and are determined by the temperature-dependent degree of solvency of the suspension liquid for the polymer. The interaction is repulsive in a good solvent and attractive in a poor solvent. For coatings whose thickness

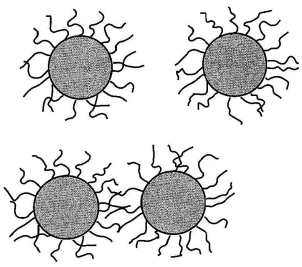

Figure 9.4: *Stabilisation of colloids with layers of polymers sticking to the surface. When the particles come close enough for the polymers to overlap, a local increase in polymer concentration leads to a repulsive force.*

is small compared to the particle radii the total polymer-polymer interaction occurs over a narrow range of interparticle spacing close to touching. In a good solvent, then, if van der Waals attractions are negligible, the effective pair potential can be approximated as that of hard spheres.

In general, the total interaction potential of sterically stabilised particles is, of course, the sum of the steric contribution and the van der Waals attraction. The latter will provide an attractive part to $V(r)$.

9.3 Equilibrium properties

The effective pair potential of suspended colloidal spheres can take on a wide variety of forms, determined by the system and the composition of the suspension medium. Typically, for a stable suspension, a hard or soft repulsion is followed by a strong or weak attraction. Qualitatively this potential is similar in form to the Lennard-Jones potential of atoms.

$$V_{\mathrm{LJ}}(r) = 4\epsilon \left[\left(\frac{\sigma}{r}\right)^{12} - 2\left(\frac{\sigma}{r}\right)^{6} \right]$$

Not surprisingly, therefore, colloidal particles in suspension can exhibit essentially the same range of phase behaviour as does a simple atomic system. However, while the pair potentials of (nonmetallic) atoms are usually assumed to be independent of temperature and density, those of colloids can vary, sometimes strongly, not only with temperature and concentration but also with other suspension conditions. For example the screening parameter κ in (9.13) in a suspension of charge stabilised colloids depends on temperature both explicitly and implicitly, through the variation of the dielectric constant ϵ, as well as on suspension ionic strength. Both van der Waals and specific coating interactions of sterically-stabilised colloids can be temperature dependent. The effective pair potential is also a strong function of any added free polymer. The simplest case to consider is the phase diagram for a hard sphere potential.

Figure 9.5: *Refractive-index-matched suspensions of PMMA spheres of radius 325 nm illuminated by white light and photographed four days after shear-melting by tumbling. Concentration, in range* $0.48 \leq \phi \leq 0.63$*, increases from right to left and samples are designated by labels 2-10 (see fig. 9.6). Sample 2 is colloidal fluid. Samples 3-5 show coexisting fluid and homogeneously-nucleated polycrystalline phases. Samples 6 and 7 are fully polycrystalline. In samples 8-10 crystallisation is heterogeneously-nucleated. Lower portions of samples 9 and 10 remained amorphous (or glassy) for many weeks. From Pusey and van Megen.*

Phase behaviour of hard spheres

Hard spheres have no critical point so that all observed behaviour is supercritical. The existence of a freezing transition of hard spheres was anticipated in early analytic work and computer simulation by calculating the free energy of the fluid phase and the solid phase. On equating (osmotic) pressures and chemical potentials for the two phases one could identifie the freezing point. At freezing the volume fractions of the coexisting fluid and solid phases were found to be $\phi_F = 0.494 \pm 0.002$ and $\phi_M = 0.545 \pm 0.002$. Recent theories and computer simulations have suggested that an assembly of hard spheres, if compressed rapidly enough to bypass crystallisation, can achieve a high-density metastable solid (or glass) state. From computer simulation studies of both thermodynamic and dynamic properties of the metastable states of hard spheres a glass transition at $\phi_G \approx 0.58 \pm 0.02$ has been identified. The first experimental study of the freezing transition of roughly hardsphere colloids of PMMA particles, gave the effective volume fraction of the crystalline phase to be about 0.51.

A more detailed study of the phase behaviour of hard-sphere colloids has been reported by Pusey and van Megen who used PMMA spheres. The particles had radii of about 325 nm. Nine samples were prepared in a range of concentration which spanned both the

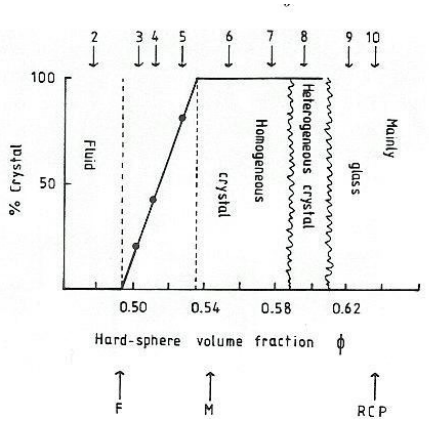

Figure 9.6: *"Phase diagram" of hard colloidal spheres, summarising behaviour seen in fig. 9.5. Numbers at top are sample designations. F, M and RCP indicate respectively the predicted freezing, melting and random-close-packed concentrations. From Pusey and van Megen.*

freezing and glass transitions. The samples were driven into metastable (or equilibrium) fluid states by slow tumbling which shear-melted any crystals present initially. They were then left undisturbed and were observed over several weeks. Figure 9.5 show the situation after four days. Because the lattice parameter of crystals of these particles is of order 0.5 μm, the crystalline phases in fig. 9.5 can be identified directly from the Bragg reflection of light. The diversity of observed phase behaviour is summarised in fig. 9.6.

The most dilute sample, 2, showed no macroscopic change with time and, presumably, is an equilibrium colloidal fluid. The next three samples, 3-5, contain coexisting colloidal fluid and homogeneously-nucleated polycrystalline phases. The fractions of the volumes of the samples occupied by the solid phase were measured. Extrapolation to 0 and to 100% crystal then provides freezing and melting concentrations. While the weight fractions of these samples can be measured accurately, it is difficult to determine the volume fractions. Thus the weight fraction at which freezing commenced was identified with an effective hard-sphere volume fraction $\phi_F = 0.494$. The volume fractions of other samples were then obtained by the appropriate scaling of their measured weight fractions. The observed melting concentration, 0.535, is somewhat lower than the expected hard-sphere value, 0.545. This difference is probably no larger than the experimental uncertainty which arises mainly from imprecise location of the fluid-solid interfaces which change with time due to slow sedimentation of the particles. Samples 6 and 7 are completely filled with small homogeneously-nucleated crystallites. No homogeneously-nucleated crystallization was observed in sample 8 but large irregular crystallites grew inwards following heterogeneous nucleation at the meniscus and cell walls. In samples 9 and 10 crystals, nucleated heterogeneously at the meniscus only, grew downwards; however the lower parts of these samples remained amorphous, i.e., glassy, for the duration, several weeks, of the observations. The glass transition concentration ϕ_G is about 0.59, in reasonable agreement with the theoretical value of $\simeq 0.58$.

Another characteristic concentration of the hard-sphere system is that of random close

packing, $\phi_{\mathrm{RCP}} \approx 0.64$. This theoretical value compares favourably with the volume fraction, $\simeq 0.66$, of the amorphous sediment formed by centrifuging samples, initially in the fluid state, rapidly enough to avoid crystallisation.

Thus the overall behaviour of this system is similar to that expected for hard spheres. Relatively small differences between experiment and theory may be associated with slight softness or attractions in the pair potential and/or polydispersity.

Structure from light-scattering

The theory for light scattering is based on the assumptions:

(i) that the intensity of light scattered by the suspension medium is negligible compared to that scattered by the particles.

(ii) that, nevertheless, the particles scatter weakly enough that only single scattering, in the first Born approximation, need be considered.

(iii) that the incident light is polarized with its electric vector perpendicular to the scattering plane.

(iv) that the individual particles are orientationally symmetrical so that the refractive index profile, $n_i(r)$, of particle i depends only on the radial distance r from the centre of the particle.

Apart from uninteresting factors the amplitude $b_i(q)$ of the field of the light scattered by particle i can be written

$$b_i(q) = 4\pi \int_0^\infty \mathrm{d}r r^2 \left[n_i(r) - n_0\right] \frac{\sin(qr)}{qr} \tag{9.15}$$

here n_0 is the refractive index of the suspension medium and $\boldsymbol{q}$ is the usual scattering vector whose magnitude q is given by

$$q = \frac{4\pi}{\lambda} \sin\frac{\theta}{2} \tag{9.16}$$

λ being the wavelength of light in the suspension and θ the scattering angle. The instantaneous amplitude $E(\boldsymbol{q}, t)$ of the field of the light scattered by an assembly of N particles is

$$E(\boldsymbol{q}, t) = \sum_{i=1}^{N} b_i(q) \mathrm{e}^{\mathrm{i}\boldsymbol{q}\cdot\boldsymbol{r}_i(t)} \tag{9.17}$$

where $\boldsymbol{r}_i(t)$ is the position of the centre of particle i at time t. The instantaneous intensity of the scattered light is given by

$$I(\boldsymbol{q}, t) = |E(\boldsymbol{q}, t)|^2 \tag{9.18}$$

and its average value by

$$\langle I(\boldsymbol{q}, t)\rangle = \sum_{i=1}^{N}\sum_{j=1}^{N} \langle b_i(q) b_j(q) \exp[\mathrm{i}\boldsymbol{q}\cdot(\boldsymbol{r}_i - \boldsymbol{r}_j)]\rangle \tag{9.19}$$

where the angular brackets indicate an ensemble average. In the case of a polycrystalline sample this includes an average over all orientations of the crystallites.

For monodisperse particles all $b_i(q)$ are the same, $b_i(q) = b(q)$. Equation (9.19) can then be written

$$\langle I(\boldsymbol{q},t)\rangle = Nb^2(0)P(q)S(\boldsymbol{q}), \tag{9.20}$$

where $P(q)$ is the (single-particle) form factor,

$$P(q) = \left[\frac{b(q)}{b(0)}\right]^2, \tag{9.21}$$

and $S(\boldsymbol{q})$ the static structure factor

$$S(\boldsymbol{q}) = \frac{1}{N}\sum_{i=1}^{N}\sum_{j=1}^{N}\langle \exp\left[\mathrm{i}\boldsymbol{q}\cdot(\boldsymbol{r}_i - \boldsymbol{r}_j)\right]\rangle. \tag{9.22}$$

Experimentally the structure factor of a monodisperse system can be determined by the following procedure: (i) a dilute suspension, for which $S(\boldsymbol{q}) = 1$ (negligible positional correlations), is prepared and its intensity $\langle I(\boldsymbol{q},t)\rangle = N_1 b^2(0)P(q)$ measured; (ii) the intensity $\langle I(\boldsymbol{q},t)\rangle = N_2 b^2(0)P(q)S(\boldsymbol{q})$ of the concentrated suspension is measured; (iii) the ratio of the second to the first measurement provides an experimental estimate of $(N_2/N_1)S(\boldsymbol{q}$.

For homogenous spheres of radius R and refractive index n_p eq. (9.15) can be evaluated to give

$$b(q) = R^3(n_p - n_0)\frac{3}{(qR)^3}\left((\sin(qR) - qR\cos(qR)\right)$$

so that (9.21) becomes

$$P(q) = \frac{9}{(qR)^6}\left((\sin(qR) - qR\cos(qR)\right)^2. \tag{9.23}$$

This form factor has a zero at $qR = 4.49$, followed by a secondary maximum of magnitude only about 0.007 at $qR = 5.76$. Because this weak scattering may be corrupted by extraneous contributions, such as background or residual multiple scattering, it is difficult to measure reliable values of $S(\boldsymbol{q})$ for $qR \geq 4$. Thus, for concentrated suspensions of hard spheres the static structure factor $S(\boldsymbol{q})$ can only be obtained reliably up to just beyond the main peak which occurs at $qR \approx 3.5$. However for dilute suspensions of interacting charged particles, where because of the large interparticle spacing, the first peak in $S(\boldsymbol{q})$ can be found at $qR < 1$, higher-order peaks can be measured with reasonable accuracy.

For polydisperse systems eq. (9.19) can no longer be simplified to the form of (9.20) since the factors $b_i(q)b_j(q)$ and $\exp\left[\mathrm{i}\boldsymbol{q}\cdot(\boldsymbol{r}_i - \boldsymbol{r}_j)\right]$ are correlated through their dependences on the particle radii R_i and R_j. Nevertheless we can define a "measured structure factor" $S_M(\boldsymbol{q})$ for a polydisperse system as the ratio of intensity scattered by a concentrated suspension to that scattered by a dilute suspension (and multiplied by the concentration ratio) i.e.,

$$S_M(\boldsymbol{q}) \quad = \quad \frac{\sum_{i=1}^{N}\sum_{j=1}^{N}\langle b_i(q)b_j(q)\exp[\mathrm{i}\boldsymbol{q}\cdot(\boldsymbol{r}_i - \boldsymbol{r}_j)]\rangle}{\sum_{i=1}^{N} b_i^2(q)}$$

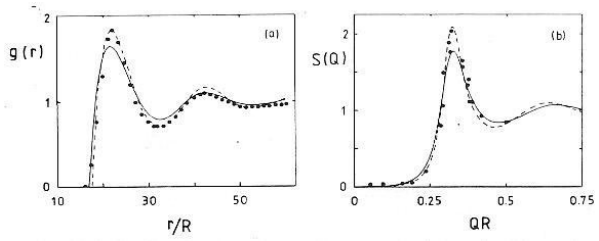

Figure 9.7: *Radial distribution function and structure factor for charged colloids of radius 23 nm and volume fraction* 4.4×10^{-4} *at low electrolyte concentration. Data points are obtained from computer simulation. The solid lines and dashed lines are theoretical results with the same potential. The mean interparticle spacing, roughly the position of the main peak in* $g(r)$*, is some eleven particle diameters for this long-ranged potential.*

$$= \frac{1}{N\overline{b^2(q)}} \sum_{i=1}^{N} \sum_{j=1}^{N} \langle b_i(q) b_j(q) \exp[\mathrm{i}\boldsymbol{q} \cdot (\boldsymbol{r}_i - \boldsymbol{r}_j)] \rangle \tag{9.24}$$

where $\overline{b^2(q)}$ is scattered intensity per particle, averaged over the particle size distribution. In general

$$\overline{b^n(q)} = \frac{1}{N} \sum_{i=1}^{N} b_i^n(q).$$

Clearly $S_M(\boldsymbol{q}) \to S(\boldsymbol{q})$ for a mono disperse system.

It has been suggested that it might, in some cases, be a reasonable approximation to neglect the correlation between scattering amplitudes and positions in a polydisperse system by "decoupling" the average in eq. (9.24):

$$S_M(\boldsymbol{q}) = \frac{1}{N\overline{b^2(q)}} \sum_{i=1}^{N} \sum_{j=1}^{N} \overline{b_i(q) b_j(q)} \langle \exp[\mathrm{i}\boldsymbol{q} \cdot (\boldsymbol{r}_i - \boldsymbol{r}_j)] \rangle \tag{9.25}$$

Since

$$\overline{b_i(q) b_j(q)} = \begin{cases} \overline{b^2(q)} & \text{for} \quad i = j \\ \overline{b(q)}^2 & \text{for} \quad i \neq j \end{cases} \tag{9.26}$$

eq. (9.25) becomes

$$S_M(\boldsymbol{q}) = (1 - x(q)) S(\boldsymbol{q} + x(q)$$

where

$$x(q) = 1 - \overline{b(q)}^2 / \overline{b^2(q)}$$

where $S(\boldsymbol{q})$ is the structure factor applying to a monodisperse system at the same number density as the polydisperse system under consideration. The decoupling approximation neglects the fact that in general there is a correlation between fluctuations in the relative concentrations of the species and fluctuations in the total number density.

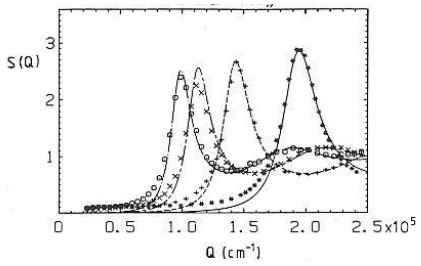

Figure 9.8: *Measured structure factors of deionised aqueous suspensions of polystyrene spheres of radius 37.5 nm. *, volume fraction* $\phi = 5.0 \times 10^{-3}$*; +,* $\phi = 2.0 \times 10^{-3}$*; x,* $\phi = 9.7 \times 10^{-4}$*; o,* $\phi = 6.4 \times 10^{-4}$*. Lines are predictions of theoretical calculations.*

From the structure factor one also obtain the pair distribution function $g(r)$ which is a direct measure of the correlation of particle positions. If n is the average number density in the suspension $ng(r)\mathrm{d}V$ is the average number of particles in a small volume element $\mathrm{d}V$ centered at a distance r from a given particle. The static structure factor is the Fourier transform of $g(r)$, i.e.

$$S(\boldsymbol{q}) = 1 + n \int \mathrm{d}\boldsymbol{r} \mathrm{e}^{\mathrm{i}\boldsymbol{q}\cdot\boldsymbol{r}}[g(r) - 1] \tag{9.27}$$

In fig. 9.7 we show the static structure factor and the corresponding radial distribution function for a charged colloidal system.

In fig 9.8 are measured structure factors for suspensions of polysterene spheres in water.

9.4 Dynamical light scattering

In order to formulate a theory of dynamical light scattering (DLS) we start with the same assumptions as were used above in the context of static scattering. When (coherent) laser light is scattered by an amorphous assembly of particles, such as a colloidal fluid, the instantaneous far-field pattern of scattered radiation constitutes a random diffraction or "speckle" pattern consisting of bright and dark regions. Each speckle subtends a solid angle $\simeq (\lambda/V^{1/3})^2$ at the sample, where ,λ is the light wavelength and V the scattering volume. The instantaneous intensity of a speckle is

$$I(\boldsymbol{q}, t) = |E(\boldsymbol{q}, t)|^2,$$

where $E(\boldsymbol{q}, t)$ is the instantaneous scattered electric field

$$E(\boldsymbol{q}, t) = \sum_{i=1}^{N} b_i(q) \mathrm{e}^{\mathrm{i}\boldsymbol{q}\cdot\boldsymbol{r}_i(t)} \tag{9.28}$$

and $\boldsymbol{q}$ is the scattering vector as before. As the particle positions $\boldsymbol{r}^N(t) = \{\boldsymbol{r}_1(t), \ldots, \boldsymbol{r}_N(t)\}$ change by Brownian motion the phase relationships determining the speckle pattern change and the pattern evolves through a sequence of random configurations.

In dynamic light scattering a detector having sensitive area roughly equal to the size of one speckle is placed in the far-field. The signal registered by the detector, proportional

to the fluctuating intensity $I(\boldsymbol{q},t)$, is fed to a photon correlator which constructs its time correlation function. Under the conditions

(i) that the scattering volume V contains a large number N of particles,

(ii) that the range of spatial correlation of the particles is much smaller than $V^{1/3}$ and

(iii) that, given enough time, the particles can diffuse throughout the suspension (Le., the system is ergodic),

it is possible to show that the field $E(\boldsymbol{q},t)$ is a zero-mean complex Gaussian variable. The factorization properties of such a variable then enable the measured (time-averaged) intensity correlation function to be written in terms of the (ensemble-averaged) time correlation function of the scattered field:

$$\langle I(\boldsymbol{q},0)I(\boldsymbol{q},t)\rangle = \langle I(\boldsymbol{q})\rangle^2 \left(1 + C\langle E(\boldsymbol{q},0)E^*(\boldsymbol{q},t)\rangle^2\right) \tag{9.29}$$

where C is an apparatus constant of order one. Dynamic light scattering thus provides an experimental estimate of the field correlation function $\langle E(\boldsymbol{q},0)E^*(\boldsymbol{q},t)\rangle$. The field (9.28) can be recognized as the instantaneous amplitude of the spatial Fourier component, having wavevector $\boldsymbol{q}$, of the refractive index fluctuations in the suspension (or, in the case of identical particles, fluctuations in the number density). With use of eq. (9.28) we can write

$$\frac{\langle E(\boldsymbol{q},0)E^*(\boldsymbol{q},t)\rangle}{\langle I(\boldsymbol{q})\rangle} = \frac{F_M(\boldsymbol{q},t)}{S_M(\boldsymbol{q})} \tag{9.30}$$

where, by analogy with the measured static structure factor $S_M(\boldsymbol{q})$ (9.24), we have defined a "measured" coherent intermediate scattering function $F_M(\boldsymbol{q},t)$ as

$$F_M(\boldsymbol{q},t) = \frac{1}{N\overline{b^2(q)}} \sum_{i=1}^{N}\sum_{j=1}^{N} \langle b_i(q)b_j(q)\exp[\mathrm{i}\boldsymbol{q}\cdot(\boldsymbol{r}_i(0) - \boldsymbol{r}_j(t))]\rangle \tag{9.31}$$

The fundamental quantity measured in a dynamic light scattering experiment is then the the corresponding normalised function

$$\Phi_M(\boldsymbol{q},t) = F_M(\boldsymbol{q},t)/S_M(\boldsymbol{q}).$$

Here $F_M(\boldsymbol{q},t=0) = S_M(\boldsymbol{q})$ and therefore $\Phi_M(\boldsymbol{q},t=0) = 1$.

For monodisperse particles, i.e. $b_i(q) = b(q)$ (9.31) becomes

$$F_M(\boldsymbol{q},t) = F(\boldsymbol{q},t) = \frac{1}{N}\sum_{i=1}^{N}\sum_{j=1}^{N} \langle \exp\left[\mathrm{i}\boldsymbol{q}\cdot(\boldsymbol{r}_i(0) - \boldsymbol{r}_j(t))\right]\rangle \tag{9.32}$$

which is the intermediate scattering function of identical particles.

It is possible to prepare a suspension which contains particles which are the same in terms of size and interactions but have slightly different refractive indices and therefore different scattering amplitudes $b_i(q)$. Then it is permissible to perform the decoupling of the average in (9.31), which was discussed above in the context of static scattering, to give

$$F_M(\boldsymbol{q},t) = \frac{\overline{b(q)}^2}{\overline{b^2(q)}} F(\boldsymbol{q},t) + \left[1 - \frac{\overline{b(q)}^2}{\overline{b^2(q)}}\right] F^s(\boldsymbol{q},t) \tag{9.33}$$

where $F^s(\boldsymbol{q},t)$ is the self intermediate scattering function

$$F^s(\boldsymbol{q},t) = \langle \exp\left(\mathrm{i}\boldsymbol{q}\cdot(\boldsymbol{r}_i(0)-\boldsymbol{r}_i(t))\right)\rangle. \tag{9.34}$$

9.5 Calculation of intermediate scattering functions

For a dilute systems of Brownian particles it is possiblew to obtain explicit expressions for the density correlation functions $F(\boldsymbol{q},t)$ and $F^s(\boldsymbol{q},t)$. We start from a Langevin equation for $\boldsymbol{r}_i(t)$, the position of particle i at time t,

$$m\ddot{\boldsymbol{r}}_i(t) = -\gamma\dot{\boldsymbol{r}}_i(t) + \boldsymbol{F}_i(t).$$

Here m is the mass of the particle and γ its friction coefficient:

$$\gamma = 6\pi\eta_0 R$$

The force $\boldsymbol{F}_i(t)$ on the particle is the sum of $\Xi_i(t)$, the rapidly fluctuating (essentially white-noise) effect of the thermal agitation of the suspension medium, and $\boldsymbol{F}_i^I(t)$, the result of direct interactions with the other particles:

$$\boldsymbol{F}_i(t) = \boldsymbol{F}_i^I(t) + \Xi_i(t).$$

The first contribution can be written

$$\boldsymbol{F}_i^I(t) = -\frac{\partial}{\partial \boldsymbol{r}_i} U\left[\boldsymbol{r}^N(t)\right]$$

where U is the effective potential of mean force.

If interparticle forces can be neglected, as in a dilute enough suspension, the results of integrating the Langevin equation was derived in chapter 4. The autocorrelation function of the velocity $\boldsymbol{v}_i$ of a free Brownian particle is given by

$$\langle \boldsymbol{v}_i(0)\boldsymbol{v}_i(t)\rangle = \frac{3k_\mathrm{B}T}{m}\exp(-t/\tau_\mathrm{B})$$

with the Brownian relaxation time

$$\tau_\mathrm{B} = \frac{m}{\gamma} = \frac{2R^2\rho_M}{9\eta_0} \tag{9.35}$$

where ρ_M is the mass density of the particle.

The mean-square displacement of a free Brownian particle is

$$\langle(\Delta\boldsymbol{r}_i(t))^2\rangle = \langle[\boldsymbol{r}_i(0)-\boldsymbol{r}_i(t)]^2\rangle = 6D_0\left[t-\tau_\mathrm{B}+\tau_\mathrm{B}\exp(-t/\tau_\mathrm{B})\right] \tag{9.36}$$

where D_0 is the "free-particle" diffusion constant

$$D_0 = \int_0^\infty \mathrm{d}t\langle \boldsymbol{v}_i(0)\boldsymbol{v}_i(t)\rangle = \frac{k_\mathrm{B}T}{\gamma}$$

The mean squared displacement has the limits

$$\langle(\Delta\boldsymbol{r}_i(t))^2\rangle = \begin{cases} \frac{k_\mathrm{B}T}{m}t^2, & t \ll \tau_\mathrm{B} \\ 6D_0 t, & t \gg \tau_\mathrm{B} \end{cases} \tag{9.37}$$

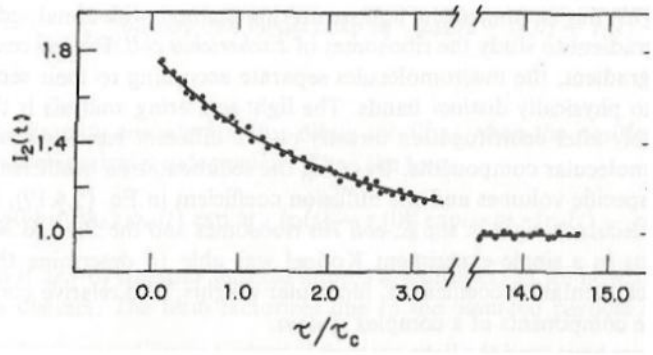

Figure 9.9: *Correlation function obtained with light scattering at a scattering angle of* 60° *for a solution containing 0.17 mg/cm*^{3} *of fd DNA in SCC (0.15 m NaCl, 0.015 m Nacitrate, pH=8) as a function of* τ/τ_c *where* $\tau_c = (q^2D)^{-1}$ *is the correlation time.* (From Newman, J., Swinney, H. L., Berkowitz, S. A. and Day, L. A. *Biochem.* **13**, 4832 (1974).)

An important conclusion can be drawn from these results. The distance moved by a typical colloidal particle in time $\tau_{\rm B}$ is very small compared to its radius. In other words, the positions of non-interacting particles in suspension change by significant fractions of their radii only in times much greater than $\tau_{\rm B}(t \gg \tau_{\rm B})$ in which their Brownian velocities have undergone many fluctuations and their motions are effectively diffusive.

In dilute suspensions where interactions between particles can be neglected we now find

$$F(\boldsymbol{q},t) \approx S(\boldsymbol{q})F^s(\boldsymbol{q},t)$$

and since $\boldsymbol{r}_i(t) - \boldsymbol{r}_i(0)$ is a Gaussian variable with mean value zero

$$F^s(\boldsymbol{q},t) = \langle \exp\left(\mathrm{i}\boldsymbol{q}\cdot(\boldsymbol{r}_i(0) - \boldsymbol{r}_i(t))\right)\rangle = \exp\left(-\frac{q^2}{6}\langle(\Delta\boldsymbol{r}_i(t))^2\rangle\right). \tag{9.38}$$

For short times we get the free-particle result

$$F^s(\boldsymbol{q},t) = \exp\left(-\frac{k_{\rm B}T}{2m}q^2t^2\right)$$

and for long times the diffusion result

$$F^s(\boldsymbol{q},t) = \exp\left(-D_0q^2t\right) \tag{9.39}$$

In fig. 9.9 we show light scattering measurements of $F(\boldsymbol{q},t)$ for highly monodisperse sample of single-stranded circular DNA from the *fd bacteriophage*, and these data can be fitted very well to the low density result in (9.39).

9.6 The Smoluchowski equation

To describe the motions of interacting Brownian particles over times measured by DLS it is sufficient to consider their configuration space distribution function $P(\boldsymbol{r}^N,t)$, where

$\boldsymbol{r}^N$ represents the set of position vectors of the N particles. An equation for P can be obtained from the Langevin equation above in the strong damping limit, and this leads to the Fokker-Planck or Smulochowski equation. A simple derivation of this equation based on a thermodynamic picture was introduced by Einstein in his study of free particle Brownian motion. A nonequilibrium distribution $P(\boldsymbol{r}^N, t)$, is prevented from relaxing by the application to each particle of a fictive force $\boldsymbol{F}_i^h(\boldsymbol{r}^N)$ derived from a potential $\Psi(\boldsymbol{r}^N)$:

$$\boldsymbol{F}_i^h(\boldsymbol{r}^N) = -\frac{\partial}{\partial \boldsymbol{r}_i}\Psi((\boldsymbol{r}^N)$$

In this hypothetical equilibrium situation $P(\boldsymbol{r}^N)$ is giyen by the Boltzmann expression

$$P(\boldsymbol{r}^N) = \text{const} \times \exp\left(-\frac{1}{k_\mathrm{B}T}\left[\Psi(\boldsymbol{r}^N) + U(\boldsymbol{r}^N)\right]\right)$$

where interparticle interactions and any external applied forces are represented by the potential $U(\boldsymbol{r}^N)$. Consequently the force $\boldsymbol{F}_i^h(\boldsymbol{r}^N)$ is given by

$$\boldsymbol{F}_i^h(\boldsymbol{r}^N) = \frac{\partial}{\partial \boldsymbol{r}_i}U(\boldsymbol{r}^N) + k_\mathrm{B}T\frac{\partial}{\partial \boldsymbol{r}_i}\ln P(\boldsymbol{r}^N)$$

The last term represents an entropy force coming from the constraints from the fictive potential.

If $P(\boldsymbol{r}^N, t)$ is now allowed to relax (the forces $\boldsymbol{F}_i^h(\boldsymbol{r}^N)$ are "switched off") a force $-\boldsymbol{F}_i^h(\boldsymbol{r}^N)$ will be driving the diffusive motion of the ith particle, We assume that a coarse-grained description of particle motion is adequate on the timescale $\tau_s \ll t \ll \tau_R$ and write

$$\boldsymbol{v}_i = -\sum_j \boldsymbol{G}_{ij} \cdot \boldsymbol{F}_i^h$$

where the $\boldsymbol{G}_{ij}$ is a generalised mobility tensor. The conservation law for the distribution P now leads directly to a generalized diffusion or Smoluchowski equation

$$\frac{\partial}{\partial t}P(\boldsymbol{r}^N, t) = -\sum_{i=1}^{N}\frac{\partial}{\partial \boldsymbol{r}_i}\cdot\left[\boldsymbol{v}_i P(\boldsymbol{r}^N, t)\right] = -L_S P(\boldsymbol{r}^N, t) \tag{9.40}$$

and

$$\begin{aligned} L_S P(\boldsymbol{r}^N, t) &= \sum_{i=1}^{N}\sum_{j=1}^{N}\frac{\partial}{\partial \boldsymbol{r}_i}\cdot\boldsymbol{D}_{ij}\cdot\left[\beta\frac{\partial}{\partial \boldsymbol{r}_j}U(\boldsymbol{r}^N)P(\boldsymbol{r}^N, t) + \frac{\partial}{\partial \boldsymbol{r}_j}P(\boldsymbol{r}^N)\right] \\ &= \sum_{i=1}^{N}\sum_{j=1}^{N}\frac{\partial}{\partial \boldsymbol{r}_i}\cdot\boldsymbol{D}_{ij}\cdot\exp\left[-\beta U(\boldsymbol{r}^N)\right]\frac{\partial}{\partial \boldsymbol{r}_j}\left\{\exp\left[\beta U(\boldsymbol{r}^N)\right]P(\boldsymbol{r}^N, t)\right\} \end{aligned} \tag{9.41}$$

where $\beta = 1/k_\mathrm{B}T$ and the diffusion and mobility tensors are related through the Einstein relation

$$\boldsymbol{D}_{ij} = k_\mathrm{B}T\boldsymbol{G}_{ij}$$

The generalized Smoluchowski equation (9.40) also determines the time dependence of $P(\boldsymbol{r}^N, t|\boldsymbol{r}_0^N, 0)$, the conditional probability that the system of particles ave the configuration $\boldsymbol{r}^N$ at time t, given that its configuration at time zero was $\boldsymbol{r}_0^N$. As

$$P(\boldsymbol{r}^N, t|\boldsymbol{r}_0^N, 0) = \prod_i \delta(\boldsymbol{r}_i - \boldsymbol{r}_{0i}) = \delta(\boldsymbol{r}^N - \boldsymbol{r}_0^N)$$

the time evolution of the system of particles can be described by the propagator

$$P(\boldsymbol{r}^N, t|\boldsymbol{r}_0^N, 0) = \mathrm{e}^{-L_S t}\delta(\boldsymbol{r}^N - \boldsymbol{r}_0^N)$$

obtained by the formal solution of (9.40).

In the case of independent particles, $U(\boldsymbol{r}^N) = 0$, we have

$$\boldsymbol{G}_{ij} = \frac{1}{\gamma}\delta_{ij}\mathbf{I}$$

where $\mathbf{I}$ is the unit dyadic, (9.40) reduces to the simple diffusion equation. This leads to the diffusion tensor

$$\boldsymbol{D}_{ij} = D_0\delta_{ij}\mathbf{I}.$$

9.7 Memory functions

A solution of the Smulochowski equation for a system of N interacting particles with N of the order of Avogadros number is not possible. Therefore one has to rely on approximations. Such approximations generally starts from a reformlation of the equations in terms of memory functions for a set of relevant dynamical variables. The derivation of the memory function is well established, and the essential steps are given below.

We consider a system described by a probability distribution in some state space of varibles $\boldsymbol{a}$ and satisfying the equation

$$\frac{\partial}{\partial t}P(\boldsymbol{a}, t) = \Omega(\boldsymbol{a})P(\boldsymbol{a}, t) \tag{9.42}$$

Here $\boldsymbol{a}$ denotes a set of state variables and Ω is some stochastic operator like the Fokker-Planck or Smoluchowski operator $\Omega = -L_S$ or possibly the Liouville operator $\Omega = -\mathrm{i}\mathcal{L}$. We will be interested in averages of some relevant dynamical variable $A(\boldsymbol{a})$ given by

$$\langle A(t)\rangle = \int \mathrm{d}\boldsymbol{a}A(\boldsymbol{a})P(\boldsymbol{a}, t) = \int \mathrm{d}\boldsymbol{a}A(\boldsymbol{a}, t)P(\boldsymbol{a}, 0) \tag{9.43}$$

Here we will consider a single variable but A could in the general case denote a column vector. $A(\boldsymbol{a}, t)$ satisfies the equation

$$\frac{\partial}{\partial t}A(\boldsymbol{a}, t) = \Omega^\dagger(\boldsymbol{a})A(\boldsymbol{a}, t) \tag{9.44}$$

and $\Omega^\dagger$ denotes the adjoint operator.

We assume that the variable A has zero equilibrium average, and we introduce a projection operator P_A defined as

$$P_A X(\boldsymbol{a}) = A(\boldsymbol{a})(\langle A^*A\rangle)^{-1}\langle A^*X\rangle; \quad \text{or} \quad P_A = \big|A\rangle(\langle A^*A\rangle)^{-1}\langle A^*\big| \tag{9.45}$$

where the asterisk denotes the complex conjugate variable. Here the bracket notation is given by

$$\begin{aligned} \langle A \mid &= \int \mathrm{d}\boldsymbol{a} A(\boldsymbol{a}) \dots \\ \mid A \rangle &= \int \dots A(\boldsymbol{a}) P_{\mathrm{eq}}(\boldsymbol{a}) \mathrm{d}\boldsymbol{a} \end{aligned} \tag{9.46}$$

where ... stands for another arbitrary function of the state variables $\boldsymbol{a}$ or in some case an operator. We will deal with a normalized variable A such that the equilibrium static correlation function is unity,

$$S = \langle A^* A \rangle = \int A^*(\boldsymbol{a}) A(\Gamma) P_{\mathrm{eq}}(\boldsymbol{a}) \mathrm{d}\boldsymbol{a} = 1 \tag{9.47}$$

In calculating the average values of the variable A only the part $P_A P(\boldsymbol{a}, t)$ enters, and we make the decomposition

$$P(\boldsymbol{a}, t) = P_A P(\boldsymbol{a}, t) + Q_A P(\boldsymbol{a}, t) = P_1(\boldsymbol{a}, t) + P_2(\boldsymbol{a}, t) \tag{9.48}$$

where $Q_A = 1 - P_A$. This leads to the coupled equations

$$\begin{aligned} \frac{\partial}{\partial t} P_1(\boldsymbol{a}, t) &= P_A \Omega P_A P_1(\boldsymbol{a}, t) + P_A \Omega Q_A P_2(\boldsymbol{a}, t) \\ &= \Omega_{11} P_1(\boldsymbol{a}, t) + \Omega_{12} P_2(\boldsymbol{a}, t) \end{aligned} \tag{9.49}$$

$$\begin{aligned} \frac{\partial}{\partial t} P_2(\boldsymbol{a}, t) &= Q_A \Omega Q_A P_2(\boldsymbol{a}, t) + Q_A \Omega P_A P_1(\boldsymbol{a}, t) \\ &= \Omega_{22} P_2(\boldsymbol{a}, t) + \Omega_{21} P_1(\boldsymbol{a}, t) \end{aligned} \tag{9.50}$$

Solving (9.50) gives

$$P_2(\boldsymbol{a}, t) = \int_0^t \mathrm{e}^{\Omega_{22}(t-s)} \Omega_{21} P_1(\boldsymbol{a}, s) \, \mathrm{d}s + \mathrm{e}^{\Omega_{22} t} P_2(\boldsymbol{a}, 0) \tag{9.51}$$

Substituting this into (9.49) gives

$$\begin{aligned} &\frac{\partial}{\partial t} P_1(\boldsymbol{a}, t) - \Omega_{11} P_1(\boldsymbol{a}, t) + \int_0^t \mathrm{d}s \hat{M}(t-s) P_1(\boldsymbol{a}, s) \\ = \;& \Omega_{12} \mathrm{e}^{\Omega_{22} t} P_2(\boldsymbol{a}, 0) \end{aligned} \tag{9.52}$$

where the operator $\hat{M}$ is given by

$$\hat{M}(t) = -\Omega_{12} \mathrm{e}^{\Omega_{22} t} \Omega_{21} = -\Omega_{12} R(t) \Omega_{21} \tag{9.53}$$

and $R(t) = \exp(\Omega_{22} t)$. Taking now the scalar product with $\langle A^* \mid$ from the left and inserting the expression for the projection operator gives the equation

$$\frac{\partial}{\partial t} \langle A^*(t) \rangle + \omega_A \langle A^*(t) \rangle + \int_0^t \mathrm{d}s M(t-s) \langle A^*(s) \rangle = \langle A^* \Omega Q R(t) Q \rangle \tag{9.54}$$

Here the frequency ω_A is given by

$$\omega_A = -\langle A^* \Omega A \rangle \tag{9.55}$$

and the memory function by

$$M(t) = -\langle A^* \Omega Q R(t) Q \Omega A \rangle \tag{9.56}$$

For the correlation function

$$C(t) = \langle A^*(t) A(0) \rangle \tag{9.57}$$

this leads to the equation

$$\frac{\partial}{\partial t} C(t) + \omega_A C(t) + \int_0^t \mathrm{d}s \, M(t-s) C(s) = 0 \tag{9.58}$$

A Laplace transformation then gives

$$C(z) = \frac{1}{z + \omega_A + M(z)} \tag{9.59}$$

Irreducible memory function

For a stochastic operator like the Smoluchowski operator Cichocki and Hess argued that (9.59) was not the best starting point for approximations on the memory function $M(z)$ since it may lead to unphysical results with a negative viscosity. They introduced an additional projection operator and obtained in this way a further reduction to an irreducible memory function $M^{\mathrm{irr}}(z)$. Later Kawasaki showed how this reduction could be generalized to a whole class of operators. A straightforward way of obtaining the irreducible memory function is to solve for $P_1(\boldsymbol{a}, t)$ in (9.49) and insert into (9.50). This gives

$$P_1(\boldsymbol{a}, t) = (\Omega_{11})^{-1} \frac{\partial}{\partial t} P_1(\boldsymbol{a}, t) - (\Omega_{11})^{-1} \Omega_{12} P_2(\boldsymbol{a}, t) \tag{9.60}$$

The "inverse" operator $(\Omega_{11})^{-1}$ is defined via

$$(\Omega_{11})^{-1} = (P_A \Omega P_A)^{-1} = -\left| A \rangle \omega_A^{-1} \langle A^* \right| \tag{9.61}$$

and satisfies

$$(P_A \Omega P_A)^{-1} (P_A \Omega P_A) = (P_A \Omega P_A)(P_A \Omega P_A)^{-1} = P_A \tag{9.62}$$

Here we assume that the inverse ω_A^{-1} exists. Equation (9.50) now reads

$$\frac{\partial}{\partial t} P_2(\boldsymbol{a}, t) - Q_A (\Omega - \Omega_0) Q_A P_2(\boldsymbol{a}, t) = \Omega_{21} (\Omega_{11})^{-1} \frac{\partial}{\partial t} P_1(\boldsymbol{a}, t) \tag{9.63}$$

where

$$\Omega_0 = \Omega P_A (P_A \Omega P_A)^{-1} P_A \Omega \tag{9.64}$$

This result was obtained by Kawasaki by splitting the operator Ω as

$$\Omega = \Omega_0 + \Omega_1 \tag{9.65}$$

where $\Omega_1 = \Omega - \Omega_0$ is the irreducible operator. We notice that $P\Omega_1 = \Omega_1 P_A = 0$ or that $Q_A\Omega_1 = \Omega_1 Q_A = \Omega_1$. Therefore the irreducible operator Ω_1 acts only in the space orthogonal to the variable A.

Solving (9.63) as before and inserting the solution in (9.49) gives

$$\frac{\partial}{\partial t}C(t) + \omega_A C(t) + \int_0^t \mathrm{d}s\, M^{\mathrm{irr}}(t-s)\frac{\partial}{\partial s}C(s) = 0 \tag{9.66}$$

The new irreducible memory function is given by

$$M^{\mathrm{irr}}(t) = \langle A^*\Omega Q R_1(t) Q\Omega A\rangle \omega_A^{-1} \tag{9.67}$$

with

$$R_1(t) = \mathrm{e}^{Q_A\Omega_1 Q_A t} \tag{9.68}$$

and the time-dependence is now given by the operator $Q_A\Omega_1 Q_A = \Omega_1$. For the Laplace transform this gives

$$C(z) = \left[z + \frac{\omega_A}{1 + M^{\mathrm{irr}}(z)}\right]^{-1} \tag{9.69}$$

From (9.59) and (9.69) one also gets the relation

$$M(z) = -\omega_A \frac{M^{\mathrm{irr}}(z)}{1 + M^{\mathrm{irr}}(z)} \tag{9.70}$$

The simple derivation above shows how the irreducible memory function can be obtained in a straightforward way by solving $P_1(t)$ in terms of its derivative from (9.49). By doing this we include the information contained in eq. (9.49) into eq. (9.50), with the effect of replacing Ω with Ω_1. The effect for the correlation function is that, instead of renormalising the frequency ω_A by $M(z)$, one rather renormalises the relaxation time by M^{irr}.

9.8 Mode-coupling approxiamtion

We are interested to calculate the intermediate scattering function $F(\boldsymbol{q}, t)$. In a first step we can find a formal expression for the corresponding memory function and then try to find some appropriate approximation.

The relevant variable is the density fluctuations

$$n(\boldsymbol{r}, t) = \sum_{i=1}^{N} \delta(\boldsymbol{r} - \boldsymbol{r}_i(t))$$

Here the delta-function picks out the positions $\boldsymbol{r}$ which are occupied by a particle in the system. The average of $n(\boldsymbol{r}, t)$ is just the mean density n in a homogeneous system. By taking the Fourier transform we find

$$n(\boldsymbol{q}, t) = \sum_{i=1}^{N} \mathrm{e}^{\mathrm{i}\boldsymbol{q}\cdot\boldsymbol{r}_i(t)}$$

and it follows that

$$F(\boldsymbol{q},t) = \frac{1}{N}\langle n^*(\boldsymbol{q},0)n(\boldsymbol{q},t)\rangle \tag{9.71}$$

i.e. the intermediate scattering function is just the density-density correlation function.

We can now choose the density $n(\boldsymbol{q})$ as the fundamental variable A and set up the memory function in the last section. This gives the formal expression

$$F(\boldsymbol{q},z) = S(\boldsymbol{q})\left[z + \frac{\Omega(\boldsymbol{q})}{1+M^{\rm irr}(\boldsymbol{q},z)}\right]^{-1} \tag{9.72}$$

We then need to calculate the frequency $\Omega(\boldsymbol{q}$ and find a more explicit expression for $M^{\rm irr}(\boldsymbol{q},z)$.

The projection operator in this case is

$$P_n = |n(\boldsymbol{q})\rangle S^{-1}(\boldsymbol{q})\langle n^*(\boldsymbol{q})| = 1 - Q_n$$

and so the frequency ω_A is

$$\Omega(\boldsymbol{q}) = \langle n^*(\boldsymbol{q})L_S n(\boldsymbol{q})\rangle / S(\boldsymbol{q}) = \omega(\boldsymbol{q})/S(\boldsymbol{q})$$

For any two dynamical variables A and B we have

$$\begin{aligned}
&\langle A(\boldsymbol{r}^N)L_S B(\boldsymbol{r}^N)\rangle \\
&= \sum_{i=1}^{N}\sum_{j=1}^{N}\int {\rm d}\boldsymbol{r}^N A(\boldsymbol{r}^N)\frac{\partial}{\partial \boldsymbol{r}_i}\cdot\boldsymbol{D}_{ij}\cdot\exp\left[-\beta U(\boldsymbol{r}^N)\right]\frac{\partial}{\partial \boldsymbol{r}_j}\left\{\exp\left[\beta U(\boldsymbol{r}^N)\right]B(\boldsymbol{r}^N)P_{\rm eq}\right\} \\
&= -\sum_{i=1}^{N}\sum_{j=1}^{N}\int {\rm d}\boldsymbol{r}^N\left\{\frac{\partial}{\partial \boldsymbol{r}_i}A(\boldsymbol{r}^N)\right\}\cdot\boldsymbol{D}_{ij}\cdot\left\{\frac{\partial}{\partial \boldsymbol{r}_j}B(\boldsymbol{r}^N)\right\}P_{\rm eq} \\
&= -\sum_{i=1}^{N}\sum_{j=1}^{N}\left\langle\left\{\frac{\partial}{\partial \boldsymbol{r}_i}A(\boldsymbol{r}^N)\right\}\cdot\boldsymbol{D}_{ij}\cdot\frac{\partial}{\partial \boldsymbol{r}_j}\left\{B(\boldsymbol{r}^N)\right\}\right\rangle
\end{aligned}$$

We will now assum that $\boldsymbol{D}_{ij} = D_0\delta_{ij}\boldsymbol{I}$. Then since

$$\frac{\partial}{\partial \boldsymbol{r}_i}n(\boldsymbol{q}) = {\rm i}\boldsymbol{q}{\rm e}^{{\rm i}\boldsymbol{q}\cdot\boldsymbol{r}_i}$$

we find $\omega(\boldsymbol{q}) = D_0 q^2$, and so

$$\Omega(\boldsymbol{q}) = \frac{D_0 q^2}{S(\boldsymbol{q})} \tag{9.73}$$

In the simplest approximation we could neglect the memory function which gives

$$F(\boldsymbol{q},z) = \frac{S(\boldsymbol{q})}{z+\Omega(\boldsymbol{q})}$$

or

$$F(\boldsymbol{q},t) = S(\boldsymbol{q}){\rm e}^{-D_0 q^2/S(\boldsymbol{q})t}$$

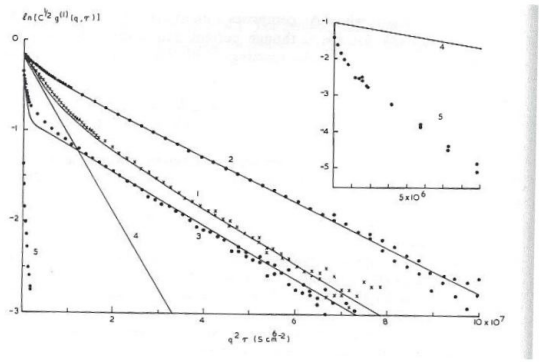

Figure 9.10: *Semilogarithmic plots of light scattering correlation functions against q^2t for polystyrene spheres of radius about 250 Å at number concentration $n \approx 2.2 \times 10^{13} cm^{-3}$ with the main peak in $S(q)$ at $q_m = 2.04 \times 1O^5 cm^{-1}$: I, $q = 3.22 \times 10^5 cm^{-1} (q > q_m)$; 2, $q = 2.12 \times 10^5 cm^{-1} (q \approx q_m)$; 3, $q = 0.89 \times 10^5 cm^{-1} (q < q_m)$; 4, "free-particle" result [equation (9.39)]; 5, data of curve 3 after subtraction of incoherent scattering*

i.e an exponential decay but with an effective q-dependent diffusion constant $D(q) = D_=/S(q)$. This approximation works very well to describe the short time dependence of F. In particular in the low-density limit where $S(\boldsymbol{q}) = 1$ it reduces to previous findings.

From measurements shown in fig. 9.10 we can extract the effective diffusion constant from the initial slope of $\ln F$ and these data can then compared with experimental values of $S(\boldsymbol{q})$.

For the irreducible memory function we have the expression

$$M^{\mathrm{irr}}(\boldsymbol{q}, t) = \langle n(\boldsymbol{q})^* L_S Q_n R_1(t) Q_n L_S n(\boldsymbol{q}) \rangle \omega^{-1}(\boldsymbol{q}) \tag{9.74}$$

A useful approximation for this memory function can be obtained if we assume that the dominant contributions to the resolvent $R_1(t)$ comes from pairs of density fluctuations, which move indepently from each other, i.e. we introduce the variables

$$A(\boldsymbol{k}_1, \boldsymbol{k}_2) = Q_n \left[n(\boldsymbol{k}_1) n(\boldsymbol{k}_2) - \langle n(\boldsymbol{k}_1) n(\boldsymbol{k}_2) \rangle \right]$$

and make the approximation

$$R_1(t) = \int \frac{\mathrm{d}\boldsymbol{k}_1 \mathrm{d}\boldsymbol{k}_2}{(2\pi)^6} |A(\boldsymbol{k}_1, \boldsymbol{k}_2)\rangle S^{-1}(\boldsymbol{k}_1) S^{-1}(\boldsymbol{k}_2) F(\boldsymbol{k}_1, t) F(\boldsymbol{k}_2, t) S^{-1}(\boldsymbol{k}_1) S^{-1}(\boldsymbol{k}_2) \langle A(\boldsymbol{k}_1, \boldsymbol{k}_2)|$$

When inserted into (9.74) we get the expression

$$M^{\mathrm{irr}}(\boldsymbol{q}, t) = \frac{D_0}{2n} \int \frac{\mathrm{d}\boldsymbol{k}}{(2\pi)^3} v^2(\boldsymbol{q}, \boldsymbol{k}) F(\boldsymbol{k}, t) F(\boldsymbol{q} - \boldsymbol{k}) \tag{9.75}$$

where the coupling coefficient $v = \langle A(\boldsymbol{k}_1, \boldsymbol{k}_2) Q_n L_S n(\boldsymbol{q}) \rangle$ can be evaluated as above and is expressed in terms of the static structure factor

$$v(\boldsymbol{q}, \boldsymbol{k}) = \hat{\boldsymbol{q}} \cdot \boldsymbol{k} n c(\boldsymbol{k}) + \hat{\boldsymbol{q}} \cdot (\boldsymbol{q} - \boldsymbol{k}) n c(\boldsymbol{q} - \boldsymbol{k})$$

where $nc(\boldsymbol{q}) = (S(\boldsymbol{q}) - 1)/S(\boldsymbol{q})$ and $\hat{\boldsymbol{q}} = \boldsymbol{q}/q$.

Therefore knowing the static structure factor we have a closed set of equations for the density correlation function which can be solved selfconsistently.

9.9 Colloidal glasses and gels

The self-consistent equations above have been used extensively to study the liquid-glass transition in colloidal suspensions and molecular glasses. In the liquid state we expect the particles to diffuse around and this eventually leads to $F(\boldsymbol{q}, t \to \infty) = 0$, while in a glass or disordered solid, the particles are trapped by surrounding particles and this leads to $F(\boldsymbol{q}, t \to \infty) = S(\boldsymbol{q})f(\boldsymbol{q}) > 0$, or $F(\boldsymbol{q}, t)$ tends to a constant. We notice that if F tends to a comnstant then also M^{irr} tends to a constant, and since $F(\boldsymbol{q}, z) \to S(\boldsymbol{q})f(\boldsymbol{q})/z, z \to 0$ and correspondingly for the memory function, the equation to determine the so called non-ergodicity parameter $f(\boldsymbol{q})$ becomes

$$\frac{f(\boldsymbol{q})}{1 - f(\boldsymbol{q})} = \frac{S(\boldsymbol{q})}{q^2} \frac{1}{2n} \int \frac{\mathrm{d}\boldsymbol{k}}{(2\pi)^3} v^2(\boldsymbol{q}, \boldsymbol{k}) S(\boldsymbol{k}) S(\boldsymbol{q} - \boldsymbol{k}) f(\boldsymbol{k}) f(\boldsymbol{q} - \boldsymbol{k}) \tag{9.76}$$

This equation always have the trivial solution $f(\boldsymbol{q}) = 0$, but there may also be nontrivial solutions for some parameter values. For systems with a hard-sphere interaction we can vary the packing fraction and solve the equation numerically. One then finds a glass transition at a packing-fraction $\phi_G = 0.52$ where there appears nontrivial solution for $f(\boldsymbol{q})$ and where the trivial solution becomes dynamically unstable.

The results for $f(\boldsymbol{q})$ obtained from (9.76) has been compared with experimental results for hard-sphere colloidal suspensions. The results are shown in fig. 9.11 and is plotted for various packing fractions or separation parameters $\epsilon = \phi - \phi_G$ versus qR. The comparison between the experimental data and the theoretical prediction is very good.

In fig. 9.12 we show corresponding values for the intermediate structure factor $F(\boldsymbol{q}, t)$ at two wavevectors, compared with the selfconsistent solution of the mode-coupling equations. Clearly the theory is in agreement with the experimental results. The major feature of the results is that when the packing fraction ϕ increases $F(\boldsymbol{q}, t)$ developes a plateau at mesoscopic times. This plateau indicates an arrest of the particles and is a precursor of the glassy state. For very high packing fractions $\phi > \phi_G$, $F(\boldsymbol{q}, t)$ seems to be constant up to the experimental time-window.

The origin of the glass transition is a self-consistent feed back mechanism. Every particle is to some extent trapped in a cage of surrounding particles, and this trapping leads to an increase of the viscosity or M^{irr} and thereby to a slowing down of $F(\boldsymbol{q}, t)$. This in turn leads to an even slower decay of the cage around every particle, and therefore also of M^{irr} which again slows down F. This feedback can eventually lead to a trapping of the particles by their surrounding particles and this leads to a glass-transition.

For hard sphere interactions the glass transition is due to the geometry of packing. A system with an interaction potential with a hard core repulsion and an attractive part shows a much richer phase diagram, and there is the possibility for other types of transitions like gelation. This mean that the glass transition switches from geometrical constraints to attraction and bonding constraints between colloidal particles.

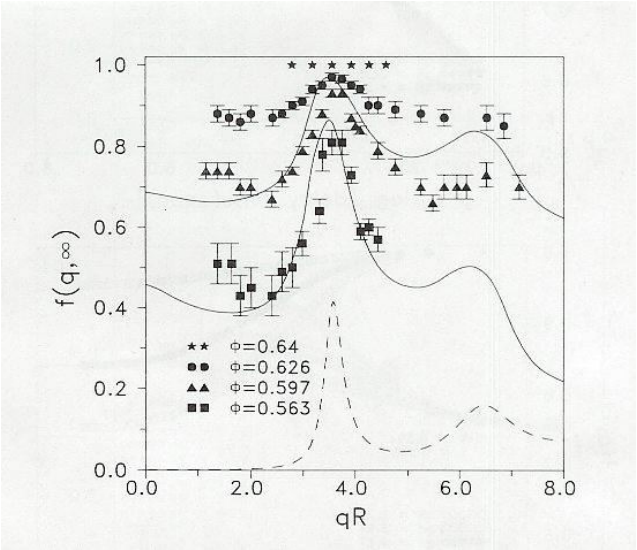

Figure 9.11: *The nonergodicity parameters $f(q)$ of hardsphere colIoidal glasses as functions of volume fraction ϕ and scattering vector. Experimental data: squares, $\phi = 0.563$, separation parameter $\epsilon \approx 0$; triangles, $\phi = 0.597, \epsilon = 0.060$; circles, $\phi = 0.626, \epsilon = 0.1l4$; stars, random-close-packed sample, $\phi \approx 0.64, \epsilon \approx 0.14$. The solid curves are the mode-coupling predictions (9.76) for the perfect hard-sphere system at separation parameters $\epsilon = 0$ (lower curve) and $\epsilon = 0.066$ (upper curve). The dashed curve is the Percus- Yevick static structure factor for hard spheres at $\phi = O.563$ reduced in magnitude by a factor of 10.*

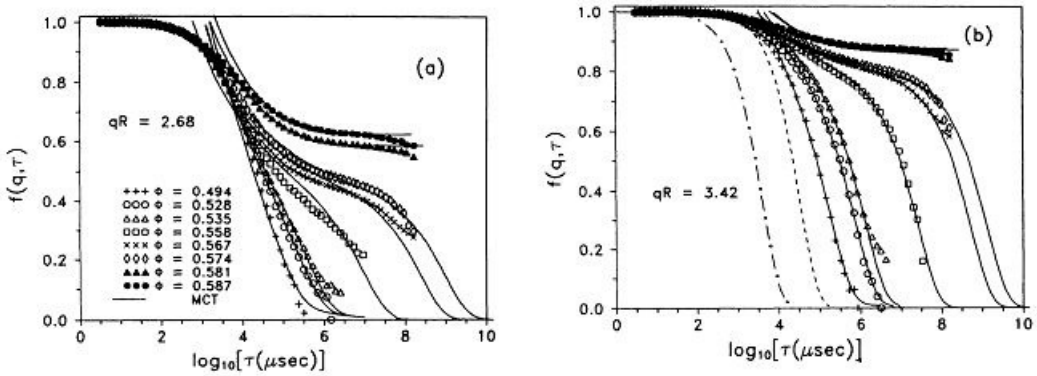

Figure 9.12: *Intermediate scattering functions for two wave vectors [(a)-(b)] around the structure factor peak. The symbols refer to the experimental data for suspension volume fractions indicated in (a). The solid curves are the MCT fits to the data. The additional curves in (b) are* $\exp[-D_0 q^2 t]$ *(—-) and* $\exp[-D(q)q^2 t]$ *(—), where D_0 is the free particle diffusion coefficient and $D(q) = D_0/S(q)$ is the shorttime collective diffusion coefficient for the colloidal fluid at freezing ($\phi = \phi_F$) at $qR = 3.42$.*

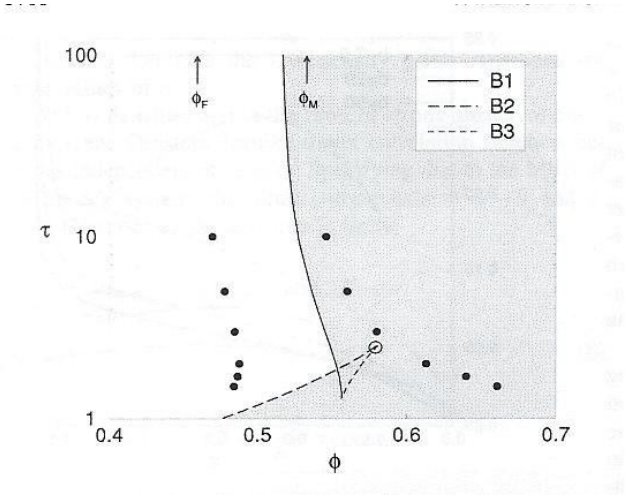

Figure 9.13: *Phase diagram in terms of the redueed temperature τ and the particle volume fraction ϕ. The labeled lines are the bifurcation lines of eq. (9.76). The shaded region enc1oses nonergodic density fluetuations. Liquid-glass transitions occur when crossing the B1 and B2 lines into the shaded nonergodie region. Also included are data for the fluid-solid freezing and melting lines (•). The arrows show the freezing (ϕ_F) and melting (ϕ_M) volume fractions for hard spheres.*

In fig 9.13 we show the phase diagram for a potential with hard sticky spheres. Except for the packing fraction there is now also an effective temperature τ which can be varied. The surprising effect is that coming from high temperatures and a glassy state there is the possibility of reentering the liquid state and then again at lower temperatures cross a new glass transition line. This is shown by the lines $B1$ and $B2$ in the figure.

This predicted reentring gelation transition have been observed in light scattering and is shown in fig. 9.14. The interaction in these experiments are varied by the addition of free polymers which effectively induces an attractive interaction between the colloidal particles.

The left part of fig. 9.14 shows the glass transition dynamics of a binary mixture of crosslinked microgel colloids with a size ratio of $R_{\text{small}}/R_{\text{large}} = 0.83$ and a number ratio $N_{\text{small}}/N_{\text{large}} = 2.65$ (corresponding to an effective polydispersity of 11 %). The density autocorrelation functions $f(q,t)$ at the peak of tbe static structure factor for volume fractions $\phi = 0.581, 0.587, 0.592, 0.595, 0.6, 0.61$ and 0.674 (from left to right) are shown. The volume fraction scale was set by mapping tbe phase behaviour of the single components to tbat of the hard sphere system. Data for samples corresponding to colloidal glasses are indicated by thick solid lines, whereas thin solid lines refer to the "supercooled" liquid state. The dashed-dotted curves correspond to fits with results of mode coupling tbeory. The glass transition volume fraction of 0.596 is found.

The right part of fig. 9.14 shows the effect on the dynamics of adding free poIymer to a colloidal glass ($\phi = 0.615$) of the binary mixture shown in left figure, demonstrating the phenomenon of a re-entrant glass transition. The density autocorre1ation curves at the

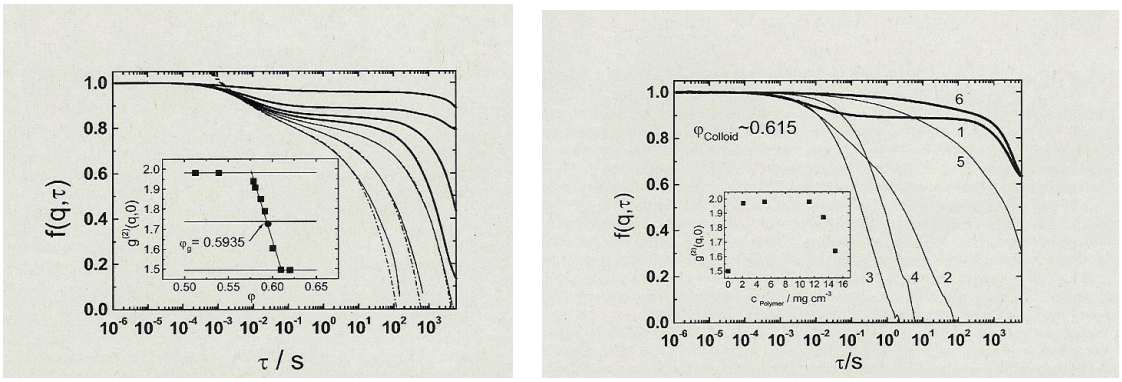

Figure 9.14: *Intermediate scattering functions for colloidal suspension with and without addition of polymers, as described in text.*

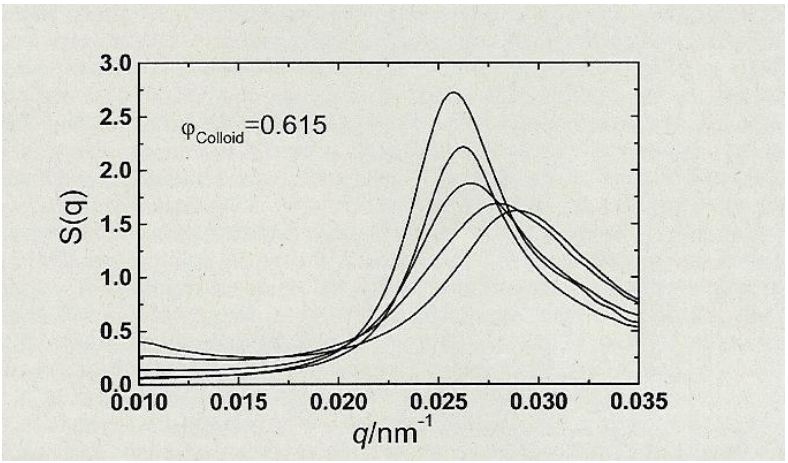

Figure 9.15: *Static structure factor for the colloidal solution with added polymers.*

peak of the static structure factor of the pure binary mixture are shown. The polymer concentrations in mg cm^{-3} (and corresponding packing fraction) increase(s) as indicated by the numbers on the curves: 1, 0 (0); 2, 2.14 (0.11); 3,5.1 (0.26); 4, 11.3 (0.57); 5, 13.3 (0.67); 6, 14.8 (0.75). Thin solid lines indicate fluid samples, whereas thick solid lines refer to glass states, as implied by the plot of the intercept values in the inset. Note the differences in the evolution of the line shapes of $f(q,t)$ on approaching the polymer-rich and the polymer-poor glass. These imply different mechanisms of glassy freezing.

The evolution of the static structure factor of the glassy binary mixture at $\phi = 0.615$ when switching on short range depletion attraction by addition of free polymer is shown in fig. 9.15. The polymer volume fractions in the free volume are (from top to bottom): 0, 0.11, 0.26, 0.57, 0.67. Note that the melting of the colloidal glass seen in fig 9.14 is accompanied by a rapid decrease in the peak maximum accompanied by a slight shift of the peak position to higher q. In contrast, the re-entrant glass transition appears to be connected to a larger shift of the peak position accompanied by a peak broadening, whereas the peak height seems to saturate. These differences can again be understood as

indications of a change in the freezing mechanism on approaching the two different glass states. The values of $S(q)$ increases at small q-values when polymers are added indicating increasing correlations on long length scales.